Electrostatic-driven self-assembled silica aerogel/tethacryloxyethyltrimethyl ammonium chloride/PMMA ternary nanocomposite with thermal insulation phase interfaces

Hongyan Li[1,2], Limeng Song[1], Yongqiang Fu[1], Cong Sun[1], Ruyi Li[1], Aiwu Yang[2,3], Hongli Liu[1,2] ✉

[1]*School of Materials Science and Engineering, Tianjin Chengjian University, Tianjin 300384, People's Republic of China*
[2]*Tianjin Key Laboratory of Soft Soil Characteristics and Engineering Environment, Tianjin 300384, People's Republic of China*
[3]*School of Civil Engineering, Tianjin Chengjian University, Tianjin 300384, People's Republic of China*
✉ *E-mail: lhlbh@163.com*

Published in Micro & Nano Letters; Received on 27th April 2018; Revised on 4th September 2018; Accepted on 24th September 2018

A three-dimensional (3D) porous silica aerogel (SA)/tethacryloxyethyltrimethyl ammonium chloride (MTC)/polymethylmethacrylate (PMMA) (SMP) ternary nanocomposite was fabricated through electrostatic-driven self-assembly by in situ polymerisation. The as-prepared products were characterised by field emission scanning electron microscopy, Fourier transform infrared spectroscopy, Zeta potential (ZETA), multi-assay gel permeation chromatography, the synchronous thermal analyser (TG), differential scanning calorimetry and so on. The results show that the ternary hybrid aerogels have an interconnected 3D nanoporous structure with a diameter of about 20–40 nm. Furthermore, positively charged MTC was successfully absorbed on the negatively charged SiO_2 aerogels surface to form high-thermal insulation phase interfaces. The SMP hybrid aerogels revealed a favourable mechanical property and an excellent thermal insulation property. Overall, the present study introduces the static electrical phase interfaces that are physical interactions between the silica phase and the polymer phase to distinctly improve the thermal insulation property of SiO_2-based aerogels, which could become a promising insulating material for broadening applications.

1. Introduction: Silica aerogels are highly porous, lightweight and good thermal insulator materials obtained by supercritical drying techniques [1–8]. Porous materials are categorised into three types based on their pore diameters which are namely: micropores, mesopores, and macropores. Moreover, porous materials with a pore diameter of <100 nm are generally named nanoporous materials [9]. Silica aerogel is one of the nanoporous materials that consistsof a three-dimensional (3D) network of silica nanoparticles [10, 11]. Aerogels are synthesised through the sol–gel [12–14] process, which can be divided into three main steps: gel preparation, aging of the gel, and drying [3]. The polymer/aerogel composites [15–17] are commonly prepared through wet mixing, dry mixing, and dual mixing [18]. Producing aerogel/polymer composites in order to enhance thermal insulating [19, 20] and mechanical properties [17, 21] of composite materials have been studied by various researchers. The thermal insulation properties of silica aerogel/epoxy composite were studied by Ge *et al.* [22]. Also, the effects of addition of aerogel nanoparticle on thermal insulation of composite were discussed. Motahari *et al.* [23] show that adding silica aerogel into polypropylene as much as 20 wt% has resulted in an increase in the thermal decomposition temperature by 24 and 34°C, supporting the increment of the thermal stability of the composites. Randall *et al.* [24] concluded that larger alkyl chains in the bis-silane improved some desired properties (low bulk density, high modulus, and recovery from compression), with the hexyl link being considered an optimum chain length. This combined approach allows, in theory, to improve the aerogels mechanical properties even further, and the open structure obtained in the silica backbone with the co-gelation of bis-silanes compensates, to some extension, the increasing density due to crosslinking. Boday *et al.* have applied surface initiated atom transfer radical polymerisation (ATRP) to grow low polydispersities poly(methyl methacrylate) on silica aerogel to prepare mechanically reinforced silica aerogel nanocomposites [25, 26]. According to their reports, the thermal insulation properties [27] and mechanical properties of as-prepared composite materials have been improved to some extent through their systematic investigation. Although the silica backbone with a chemically bonded polymer for increasing mechanical strength is an effective way, whether the thermal insulation of aerogels could decrease is still unknown. Hence, electrostatic interactions between the silica phase and polymer phase exhibit high interfacial thermal resistances, and the heat flux could be held in the silica phase. This has been reported in previous work by us [28].

In the study, the SA/polymer composites were prepared successfully through electrostatic interaction by loading the positively charged tethacryloxyethyltrimethyl ammonium chloride (MTC). After that, the MTC with a high thermal insulation phase interface [29–31] was constructed between the silica phase and the PMMA [32, 33] phase. The high thermal insulation through electrostatic interaction was studied. Meanwhile, the microstructure morphology and thermal stability of composites were analysed. The construction of phase interfaces and the mechanisms of phase interfaces on the reinforcement and thermal conductivity [34, 35] of the composites were investigated. Furthermore, we further investigated the glass transition temperature (T_g) [36] of the polymers phase, the effect of the MTC on the molecular weight and molecular chains movement of composites (Fig. 1).

2. Experimental

2.1. Materials: Tetraethyl orthosilicate (TEOS, chemically pure) was purchased from Sigma-Aldrich, USA. Benzoyl peroxide (BPO, analytical reagent) was obtained from Aladdin Industrial Corporation (Shanghai, China). Tethacryloxyethyltrimethyl ammonium chloride (MTC, analytical reagent) was purchased from Dow Corning Corporation. Other reagents were all of analytical reagents.

2.2. Preparation of materials

2.2.1. Preparation of SiO_2 aerogels (SA): The precursor solution was obtained by mixing TEOS, ethanol and deionised water with

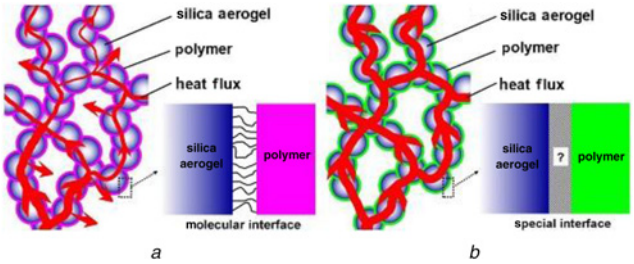

Fig. 1 *Heat flux in SA/polymer composites with different phase interfaces [28]*
a Covalent bond phase interface
b Electrostatic interaction phase interface

a molar ratio of 1:8:3.75, respectively. Hydrochloric acid was added into the precursor solution, pH value was adjusted to 3–4, and the mixture was stirred with magnetic stirring apparatus for 60 min to make it evenly mixed. The mixture solution was hydrolysed at a constant temperature for 16 h, then 0.5 mol/l ammonia solution was added to adjust pH value to 7–8. The mixture was stirred until forming a gel, ethanol solution was added and aged for 24 h at 60°C. Then wet gels of SiO_2 were obtained through n-hexane solvent replacement for three times (one time about 3 h) and SA could be obtained through CO_2 supercritical drying [37].

2.2.2. Synthesis of polymers: The polymers were synthesised through the copolymerisation method using methylmethacrylate (MMA) and MTC as the monomer. The PMMA/MTC copolymers were prepared as follows: first, 10 g MMA and 0.55 g MTC (mass fraction of 75%) were mixed and then 0.07 g BPO was added to the mixture under magnetic stirring. The mixture was heated up to 85°C and maintained for 45 min until the prepolymer became sticky, and controlled quickly the temperature at about 40°C with cooling water. The PMMA/MTC copolymer materials were obtained by allowing the prepolymer to stand until all the bubbles were removed. For comparison, the PMMA polymer was also synthesised by the same method. What is more, the positively charged MTC monomers have strong electrostatic repulsion with each other, therefore, they are not easy to copolymerise, so it was named as MTC.

2.2.3. Preparation of hybrid aerogels: The prepared SA (0.2 g) was added into 10 ml distilled water and 0.01 g MTC was added dropwise into the mixture under ultrasonication for 1 h to make it evenly mixed. Then the mixture was dried in an oven for 5 h at 80°C and the electrostatic SA/MTC binary hybrid aerogel was prepared. The SA/PMMA binary hybrid aerogel was obtained from SA and MMA monomer using the same method. In order to ensure the preparation of the favourable insulation property, the weight ratio of SA, MMA, and MTC was 10:96:4. After ultrasonication at room temperature, the solution was transferred into a 50 ml teflon-sealed autoclave and reacted at 100°C for 12 h. The as-obtained hydrogel was collected, washed with deionised water several times, and samples were placed inside the supercritical device in the condition 35°C and 8 MPa, and they were kept in this condition for two days. The supercritical device was under surveillance to ensure that the constant temperature and pressure in the supercritical CO_2. Afterwards, samples were removed from the supercritical device.

2.3. Characterisation: The sizes and morphologies of as-prepared samples were determined by scanning electron microscopy (SEM; Nanosem 430, FEI company, USA). The determination of the materials of the groups was performed through Fourier transform infrared (FTIR) spectroscopy (Thermo Nicolet 380, Thermoelectri Corporation, USA). Before FTIR measurements, all samples were Soxhlet extracted with refluxing ethanol for 48 h, then dried at 80°C to remove the ethanol. The samples were characterised on a powder X-ray diffraction (XRD) analyser (PW1830, Philips) with CuKα radiation ($\lambda = 0.154$ nm) at a generator voltage of 40 kV and a generator current of 40 mA with a scanning speed of 10°/min from 10° to 60°. Zeta potential values of SA and composites were measured by using a Brookhaven Zetasizer (Brookhaven Instruments Ltd, USA). The composition of the materials was qualitatively analysed by using a synchronous thermal analyser (DTU-2B, TG, Beijing Boyuan Precision Technology Development Corporation). The molecular weight and molecular weight distribution of polymers were tested by using a multi-assay gel permeation chromatography (TDA305, Malvern, UK). The glass transition temperature and thermal stability of as-prepared materials were analysed by using a differential scanning calorimeter (DSC1, DSC, Beijing Hengjiu Chemical Instrument Factory, China) (Table 1).

3. Results and discussion

3.1. Morphology of aerogels: The surface morphology of the modified silica aerogel 3D network structure was performed by electron microscopy. Fig. 2 shows SEM images of SA and SMP. As shown in Fig. 2*a*, SiO_2 nanoparticles of aerogel are spherical in shape with diameter around 10–20 nm. The SA presents interconnected frameworks with a 3D porous spongy structure. In Fig. 2*b*, the bright field is the composite particles with the similar size of 20–40 nm, the dark field is the pore in the composite structure, suggesting an efficient hybrid between the SA and polymers through the electrostatic interaction. The composite particles size and the pores size are larger than that of SA. It can be seen that a 3D nano-size porous network is interconnected and formed, suggesting that the 3D block was a good porous spongy structure.

3.2. As-prepared products testing: The FTIR spectra of (A) SA, (B) PMMA, (C) MTC, (D) SA/MTC, (E) SA/PMMA, (F) PMMA/MTC and (G) SMP are illustrated in Fig. 3. As shown in (A) spectra, an absorption peak appearing at 3523 cm^{-1} is relative to stretching vibration of the –OH group on the surface of the SA sample. The peaks at about1088, 848 and 472 cm^{-1}

Table 1 Composition

Sample	Reaction ratio, wt%		
	SA	MMA	MTC
SA	100	0	0
PMMA	0	100	0
MTC	0	0	100
SA/MTC	100	0	4
SA/PMMA	10	100	0
PMMA/MTC	0	96	4
SMP	10	96	4

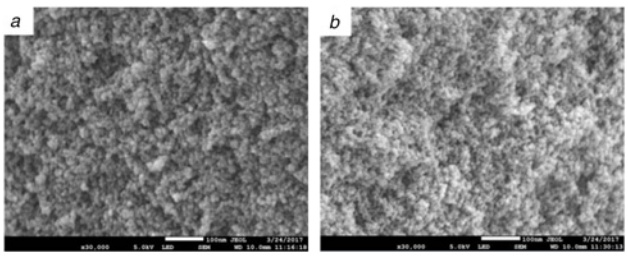

Fig. 2 *SEM images of*
a SA
b SMP

doi: 10.1049/mnl.2018.5099

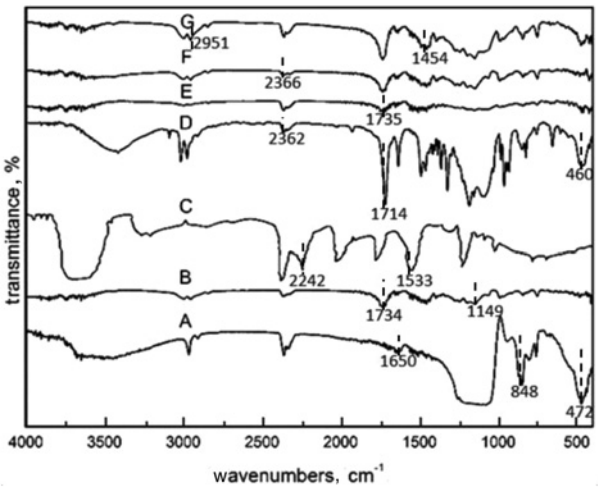

Fig. 3 *FTIR spectra of (A) SA, (B)PMMA, (C) MTC, (D) SA/MTC, (E) SA/PMMA, (F) PMMA/MTC and (G) SMP*

are associated with stretching vibration of Si–O–Si. The broad peak in the range of around 1650 cm^{-1} is due to the absorbed water molecules. The spectrum of PMMA (Fig. 3B) absorption peak appears at 1734 cm^{-1} because of stretching vibration of ester groups (C=O). The peaks at 1458 and 1396 cm^{-1} are relative to stretching vibration of SP^2 and SP^3 hybrid hydrogen bond of C–H groups, respectively. The intense peaks at 1241 and 1149 cm^{-1} are the characteristic peaks for C–O–C. Fig. 3(C) shows intense absorption bands at about 3207 and 3266 cm^{-1} because of stretching vibration of C–H groups of $–CH_3$. The peak at 2379 cm^{-1} is relative to stretching vibration of C=O groups. The absorption bands at 2242 cm^{-1} is the characteristic peak for C=C groups. The peak at 2033 cm^{-1} is relative to stretching vibration of $–(CH_2)_2$. Absorption peaks appearing at 1533 and 1778 cm^{-1} are associated with stretching vibration of C–O groups. The peak at 1230 cm^{-1} is relative to stretching vibration of $N^+(CH_3)_3$ groups. It is obvious that in the spectrum of the SA/MTC (Fig. 3D), the absorption peak appearing at 2362 cm^{-1} is related to stretched vibration of C=O groups. The peak at around 2329 cm^{-1} is ascribed to C=C groups. Absorption peaks appearing at 1633 and 1714 cm^{-1} are associated with the bending vibration of C–O–C groups. A sharp absorption peak appears at 1227 cm^{-1} due to the stretching vibration of $N^+(CH_3)_3$ groups and the peaks at 1182, 832 and 460 cm^{-1} are ascribed to the Si–O–Si groups. It showed that the SA/MTC samples have groups of SA and MTC. As shown in Fig. 3E spectra, the absorption peak appearing at 1735 cm^{-1} is associated with stretching vibration of C=O groups. The peaks around 1145 and 843 cm^{-1} are attributed to stretching vibration of Si–O–Si groups. It could be observed in the absorption peaks of curve (E) have C=O groups compare with the curve (A), suggesting the MMA successfully grafted on the SA surface. The C=C groups were not found in the absorption peaks of curve (E), showing no unpolymerised MMA monomers in composite and the polymer chains has no obvious influence when SA was added into the system. Fig. 3F, absorption peaks appearing at about 2366 and 1731 cm^{-1} because of stretching vibration of C=O groups. The peaks at about 1149 cm^{-1} are relative to stretching vibration of C–O–C groups. The C=C was not found in the absorption peaks of curve F, suggesting the polymerisation process is thorough. The spectrum of SMP (Fig. 3G) absorption peaks appear at 3001 and 2951 cm^{-1} because of stretching vibration of C–H. The peaks at 2361 cm^{-1} are relative to stretching vibration of C=O groups. The intense peak at 1734 cm^{-1} is the characteristic peak for C–O. The peak at around 1454 cm^{-1} is attributed to stretching vibration of CH_2 groups. The peak at around 1241 and 1147 cm^{-1} are attributed to stretching vibration of C–O–C groups. The peaks at 844 and 474 cm^{-1} are ascribed to the Si–O–Si groups. The absorption peak appearing at 1735 cm^{-1} is associated with stretching vibration of $N^+(CH_3)_3$ groups. The groups of SA, MMA, and MTC except C=C were all found in the absorption peaks of curve (G), suggesting the polymers were loaded the aerogels framework through electrostatic attraction.

3.3. Materials XRD measurement: Fig. 4 shows the X-ray diffraction pattern of the SA, PMMA, SA/PMMA, PMMA/MTC, and SMP composite. The XRD pattern of SA shows a wide peak at −23.3° which corresponds to the amorphous matrix of SiO_2, showing lack of crystallinity in its structure. The XRD pattern of PMMA shows two peaks, the first intense peak at 13.8° reflects the ordering of the PMMA chain while the second peak at 29.9° reflects the ordering within the main chain. The XRD pattern of SA/PMMA shows the absence of the SA peak could be attributed to the intense peak of PMMA, which overshadowed the typical peak of silica at 28.8°. On the other hand, the characteristic peaks of PMMA/MTC also show typical PMMA reflection peaks at 13.8° and 29.4°. The red shift of the peaks and the change in the intensities compared with that of PMMA indicated the ordering of the polymer main chain decreased. Thus, SA and MTC components as inhibitors reduce ordering of the PMMA. It should be noted that the peak at 27.1° of the SMP, the red shift of the peak is more obvious than that of other PMMA-based composites, which can be ascribed to the synergistic effect of SA and MTC.

3.4. Zeta potential values measurement: Fig. 5 shows zeta potential values of SA, PMMA, MTC, SA/MTC, SA/PMMA, PMMA/MTC, and SMP. The measurements were performed at room temperature with a pH value of 7. As shown in Fig. 5, the zeta potential value of the SA sample is about −38.61 mV. This could be due to the dislocation of silanol groups on the surface of SA and would form SiO^-. The zeta potential value of the PMMA sample is almost 0. The MTC sample with positively charged $–N^+(CH_3)_3$ groups obtained a zeta potential value of 54.63 mV. It is obvious that SA/MTC shows a 1.2 mV because of charge neutralisation of two phases and only 4% MTC was contained in the solution, in which the amount of charge was small. The SA/PMMA sample reveals a zeta potential value of about −22.35 mV due to the negatively charged SA component of the composite. The PMMA/MTC copolymer sample got a zeta potential value of around 24.43 mV and could be attributed to the $–N^+(CH_3)_3$ groups with a positive charge in the second monomer MTC. It is can be seen that the zeta potential of the SMP composite is about −17.95 mV, which lies between those of SA and copolymer. This could be because the positive charges of $–N^+(CH_3)_3$ groups were neutralised by the negative ones on dissociated SiO^- groups, with the incorporation of the SA phase. This phenomenon further

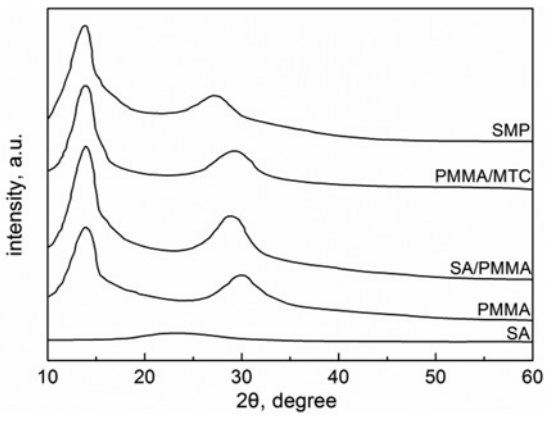

Fig. 4 *XRD patterns of the SA, PMMA, SA/PMMA, PMMA/MTC, and SMP composite*

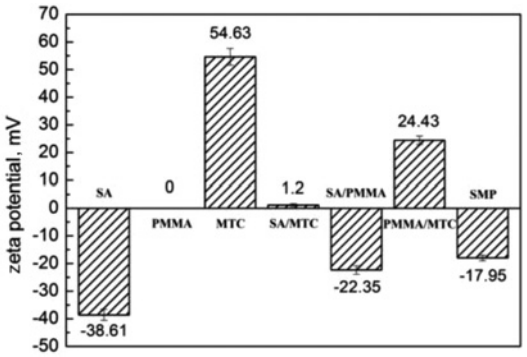

Fig. 5 *Zeta potential of SA, PMMA, MTC, SA/MTC, SA/PMMA, PMMA/MTC, and SMP*

determined that the chain of the PMMA/MTC copolymer adsorbed effectively onto the SA skeleton surface, and the electrostatic interaction between SA and copolymer phases has taken place.

3.5. Effects of polymers on the molecular weight: Fig. 6 shows a graph of molecular weights of PMMA, SA/PMMA, PMMA/MTC, and SMP. The polydispersity index of the polymer is often expressed by D (M_w/M_n). The larger the D and the wider the molecular weight distribution. As shown in Fig. 5, the M_n of the SA/PMMA sample (1.37×10^5) is less than that of the PMMA sample (2.13×10^5), it could be attributed to the nano-size pores of the SA phase inhibit monomers diffusion. When MMA monomers contacted the SA skeleton surface, the free radical active point could disappear. The PMMA further radical polymerisation may be prevented. Furthermore, the monomers inside the pores could not be effectively polmerised with the other location, the low molecular weight polymer increased. However, the M_n of PMMA/MTC is 2.29×10^5, which is larger than that of PMMA. On the one hand, the molecular weight of the MTC monomer (207.7) is around twice than that of MMA monomer (100.12) and it could lead to increase the molecular weight of the copolymer. On the other hand, the MTC and MMA monomers copolymerised through the double bond to form a copolymer, MTC molecular chains would be mutually exclusive and the movement space became large, which could promote a further polymerisation. The M_n of the SMP sample is 1.39×10^5. It is less than that of PMMA/MTC and slightly larger than that of SA/PMMA. It suggested that SA played a greater role than that of MTC during polymerisation reaction. The polydispersity index of SA/PMMA is 3.03, which is larger than that of PMMA (2.32). The reason for that MMA could be adsorbed to the pores of SA, the MMA in the pores could be polymerised, and the other location could not be polymerisation. The PMMA radical polymerisation could be hindered. Another reason was that when

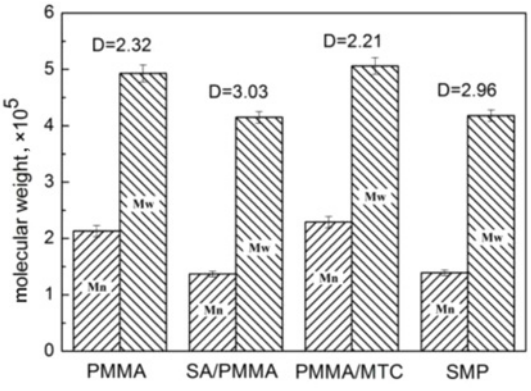

Fig. 6 *Molecular weight of polymers and composites*

the PMMA was absorbed onto the SA surface, the free radical active point disappeared, the SA acted as a polymerisation inhibitor. The polydispersity index of PMMA/MTC (2.21) is lower than that of the PMMA sample (2.32). The reason was that MTC has positive charges, SA has negative charges, MTC molecular chains would be mutual exclusive and the movement space became large. Based on the above analysis, it could be inferred that the polydispersity index of samples decreased by adding positively charged MTC monomers, however, the polydispersity index increased through introducing SA. Therefore, the polydispersity index of SMP (2.96) is lower than that of SA/PMMA and larger than that of PMMA/MTC.

3.6. Materials thermogravimetric analysis (TGA) testing: Fig. 7 shows the TGA curves of PMMA, SA/PMMA, PMMA/MTC and SMP samples at a heating rate of 20°C/min. The samples were heated from room temperature to 500°C under air atmosphere. According to the TGA results, the onset temperature (T_0) and temperature at a weight loss of 50% (T_{50}) of the samples are summarised in Table 2. T_0 and T_{50} of samples are typical parameters for reflecting their thermal stability. The PMMA sample started decomposing when the temperature continuously increased to 251°C in the air atmosphere. The essence of that molecular chains of polymer fracture appears at higher temperature [38]. The weight reduced by almost 100% when the temperature increased to 387°C. It suggested pure PMMA has been wholly decomposed more than this temperature. This is similar to PMMA when the temperature was raised to 263°C, the PMMA/MTC started decomposing. The weight of the sample was wholly decomposed when the temperature increased more than 392°C. Moreover, the T_{50} value of the PMMA/MTC sample is 326°C, which is slightly higher than that of the PMMA sample. This could be MMA monomers and the positively charged MTC monomers copolymerised to form the long chain. MTC monomers would exhibit electrostatic repulsion and the movement space became large to promote a further polymerisation. The thermal stability is improved due to the longer molecular chain and larger molecular weight. However, decomposition temperature was not improved markedly attributed

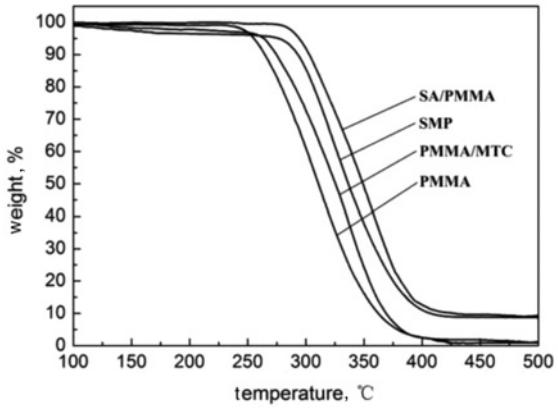

Fig. 7 *TGA curves of polymers and composites*

Table 2 TGA and DSC data of PMMA and composites

Sample	T_0, °C	T_{50}, °C	T_g, °C
PMMA	251	311	113
SA/PMMA	290	349	120
PMMA/MTC	263	326	105
SMP	285	336	108

doi: 10.1049/mnl.2018.5099

to the MTC monomers were introduced only 4wt%. The T_{50} of SA/PMMA sample (349°C) is larger than that of PMMA (311°C), suggesting thermal stability is improved through an efficient assembly between an inorganic phase and an organic phase. The polymer chains degradation were inhibited by introducing the inorganic phase. The T_{50} value of the SMP sample (336°C) is higher than that of the PMMA/MTC sample, nevertheless, it is lower than that of the SA/PMMA sample. The polymer phase degradation of SMP is consistent with that of the SA/PMMA sample. Nano-size porous SA acted as an inhibitor, which would inhibit polymer chains decomposed. As we known, the thermal stability of a material is affected by its thermal conductivity. The copolymer was attracted to the SA surface to form an electrostatic interaction phase interface [29] between the SA phase and the polymer phase. The static electrical phase interfaces that are physical interactions are with high interfacial thermal resistances. Therefore the heat flux in materials was not easy to get a balance in a high-temperature environment. Local high temperature zones in this composite will appear, and the thermal stability would decrease.

3.7. Materials differential scanning calorimetry (DSC) measurement: Fig. 8 shows the DSC curves of PMMA, SA/PMMA, PMMA/MTC and SMP samples at a heating rate of 5°C/min. The samples were heated from room temperature to 220°C under air atmosphere. According to the DSC results, the glass transition temperature (T_g) [39] of the samples are summarised in Table 2. Since silica aerogel nanoparticles do not bear any transitions in this range of temperature, therefore only the thermal transition of copolymers is observed. As shown in Table 2, the T_g value of the PMMA (113°C) is lower than that of SA/PMMA (120°C) because some of the molecular chains were adsorbed into the pores, it could limit the movement of the molecular chains, groups etc., and the glass transition temperature increases. The T_g value of the PMMA/MTC is 105°C, which is lower than those of other samples. It may be the positively charged MTC and MMA monomers copolymerised to form a charged macromolecular copolymer. Therefore, the movement space is large within long chains of the copolymer because of electrostatic repulsion. Meanwhile, it could leadto increase chain segment mobility and decrease T_g values. The T_g value of the SMP sample is 108°C, which is larger than that of PMMA/MTC and lower than that of SA/PMMA samples. This is an explanation that the 3D nano-size porous structure of SA inhibits chain segment migration, which results in increase in T_g. The movement space between long chains was extended through electrostatic interaction, which results in T_g reduction.

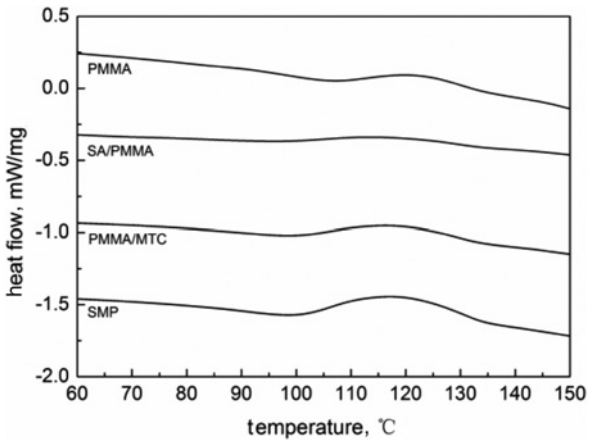

Fig. 8 *DSC curves of polymer and composites*

3.8. Multifunctional properties of as-prepared materials: The Brunauer Emmett and Teller (BET) surface areas, average pore diameters, compressive strength and thermal conductivity of as-prepared samples are calculated and listed in Table 3. According to the data of Table 3, it is obviously seen that the BET surface area of SMP is 432.59 m^2/g. The average pore diameter of the SMP sample is 28.32 nm. However, the SA/PMMA BET surface area is 218.37 m^2/g and the average pore diameter is 32.58 nm. It can be interpreted that the positively charged MTC was successfully absorbed on the negatively charged SA surface. The 3D pore structure of the ternary hybrid aerogel was extended through electrostatic interaction. Meanwhile, it can also be found that the average pore diameters of SMP are larger than that of SA because the polymers were introduced into the SA phase. The results are consistent with that of SEM analysis.

As shown in Table 3, the compressive strength of SA is too weak to detect. The pure PMMA sample obtained a compressive strength of about 112.19 MPa. The compressive strength of the copolymer is increased through adding an MTC monomer. The reason may be the MTC could promote MMA polymerisation, which make the M_n of the copolymer large. Therefore, PMMA/MTC got a compressive strength of around 128.35 MPa. The compressive strength of SA/MTC is similar to that of SA. The reason that MTC monomers just absorbed on the negatively charged aerogels framework through electrostatic interaction and they cannot polymerise each other. The compressive strength of SA/PMMA is 0.86 MPa. Furthermore, the compressive strength of SMP is about 2.75 MPa. This may be related to the MTC and MMA monomers copolymerised through the double bond to form copolymers. The copolymer and SA formed a monolithic through electrostatic interaction to improve SMP compressive strength. It is noted here that the MTC as a stable phase interfaces between the PMMA phase and the SA phase, which is an efficient load transfer medium, and the compressive strength is further improved.

In Table 3, SA as a super thermal insulation material got a thermal conductivity of about 0.022 W/(m·K), the thermal conductivity of SA/PMMA is 0.121 W/(m·K) and the thermal conductivity of PMMA is around 0.213 W/(m·K). However, the thermal conductivity of SMP hybrid aerogel is 0.056 W/(m·K), which is lower than that of SA/PMMA. It could be associated with the MTC and was absorbed onto the SA surface to form an electrostatic interaction phase interface [29], therefore the thermal conductivity decreased. Likewise, the results are consistent with the results of the TGA.

Table 3 Multifunctional properties of as-prepared samples

Sample	BET surface area, m^2/g	Avera-ge size, nm	Compressi-ve strength, MPa	Thermal conductivit-y, W/(m·K)
SA	529.98	13.07	—	0.022
PMMA	—	—	112.19	0.213
SA/MTC	479.13	20.19	—	—
SA/PMMA	218.37	32.58	0.86	0.121
PMMA/MTC	—	—	128.35	0.215
SMP	432.59	28.32	2.75	0.056

'—' The properties of the sample cannot be measured reliably.

4. Conclusion: The composite aerogels with polymers as reinforcement were successfully prepared through the sol–gel method combined with supercritical drying. The as-prepared materials were characterised by SEM, TGA, DSC, BET and so on. The results indicated that SMP has a porous and spongy structure, with average pore diameters around 28.32 nm. The SMP specific surface area was as large as 432.59 m^2/g, which is larger than that of SA/PMMA (218.37 m^2/g) as MTC was successfully grafted onto the SA surface through electrostatic interaction. The SMP ternary hybrid aerogels framework through loading the copolymer revealed an excellent compressive strength of about 2.75 MPa. The thermal conductivity of SMP is 0.056 W/(m·K), which is lower than that of SA/PMMA (0.121 W/(m·K)), suggesting it obtained a better thermal insulation property. DSC results suggested that the T_g value increased as SA inhibits chain segment migration and the T_g value decreased because copolymer extends the movement space between long chains. On the basis of the above results, it could be inferred that the electrostatic interaction phase interface with high thermal insulation was formed and the copolymer was strong enough for supporting aerogel materials.

5. Acknowledgment: This work was financially supported by the National Natural Science Foundation of China (grant nos. 51503141 and 51772202) and the Natural Science Foundation of Tianjin (grant no. 18JCQNJC03000).

6 References

[1] Gurav J.L., Jung I.K., Park H.H., *ET AL.*: 'Silica aerogel: synthesis and applications', *J. Nanomater.*, 2010, **409310**, pp. 1–11
[2] Duraes L., Ochoa M., Rocha N., *ET AL.*: 'Effect of the drying conditions on the microstructure of silica based xerogels and aerogels', *J. Nanosci. Nanotechnol.*, 2012, **12**, pp. 6828–6834
[3] Soleimani Dorcheh A., Abbasi M.H.: 'Silica aerogel; synthesis, properties and characterization', *J. Mater. Process. Technol.*, 2008, **199**, pp. 10–26
[4] Cai J.Y., Lucas S., Wang L.J., *ET AL.*: 'Insulation properties of the monolithic and flexible aerogels prepared at ambient pressure', *Adv. Mater. Res.*, 2011, **391–392**, pp. 116–120
[5] Yaprak O., Zeynep U., Can E.: 'Monolithic composites of silica aerogel with poly(methyl vinyl ether) and the effect of polymer on supercritical drying', *J. Supercrit. Fluids*, 2015, **105**, pp. 108–118
[6] Mark D., Michael G., Tim B., *ET AL.*: 'Streamlined life cycle assessment of transparent silica aerogel made by supercritical drying', *Appl. Energy*, 2012, **97**, pp. 396–404
[7] Wu R.L., Nie X.D., Du J., *ET AL.*: 'Preparation of amphoteric nanocomposite hydrogel under supercritical carbon dioxide and its fast-swelling behaviours', *Int. J. Nanotechnol.*, 2017, **14**, pp. 457–469
[8] Scanlon S., Aggeli A., Boden N., *ET AL.*: 'Peptide aerogels comprising self-assembling nanofibrils', *Micro Nano Lett.*, 2007, **2**, pp. 24–29
[9] Cabañas A., Enciso E., Carbajo M.C., *ET AL.*: 'Synthesis of SiO_2-aerogel inverse opals in supercritical carbon dioxide', *Chem. Mater.*, 2005, **17**, pp. 6137–6145
[10] Bandi S., Bell M., Schiraldi D.A.: 'Temperature-responsive clay aerogel–polymer composites', *Macromolecules*, 2005, **38**, pp. 9216–9220
[11] Hwang S.W., Kim T.Y., Hyun S.H.: 'Effect of surface modification conditions on the synthesis of mesoporous crack-free silica aerogel monoliths from waterglass via ambient-drying', *Microporous Mesoporous Mater.*, 2010, **130**, pp. 295–302
[12] Agnieszka S.: 'Recent advances in research on the synthetic fiber based silica aerogel nanocomposites', *Nanomaterials-Basel*, 2017, **7**, p. 44
[13] Alireza D., Cinzia B., Elisa B., *ET AL.*: 'Preparation and characterization of polyurethane/silica aerogel nanocomposite materials', *J. Appl. Polym. Sci.*, 2017, **134**, p. 44521
[14] Vekariya R.L., Dhar A., Lunagariya J.: 'Synthesis and characterization of double $-SO_3H$ functionalized Brönsted acidic hydrogensulfate ionic liquid confined with silica through sol-gel method', *Compos. Interfaces*, 2017, **24**, pp. 801–881
[15] Mohammadreza S., Kaveh K., Khezrollah K.: 'SR&NI atom transfer radical random copolymerization of styrene and butyl acrylate in the presence of MPS-functionalized silica aerogel nanoparticles', *J. Therm. Anal. Calorim.*, 2016, **126**, pp. 1261–1272
[16] Khezrollah K., Yousef F.: 'Synthesis and characterization of poly (styrene-co-butyl acrylate)/silica aerogel nanocomposites by in situ AGET ATRP: investigating thermal properties', *High Temp. Mater. Process.*, 2017, **36**, pp. 955–962
[17] Navid E., Siamak M., Zhale A., *ET AL.*: 'Thermal, mechanical, and acoustic properties of silica-aerogel/UPVC composites', *J. Appl. Polym. Sci.*, 2017, **134**, p. 44685
[18] Kim G., Hyun S.: 'Effect of mixing on thermal and mechanical properties of aerogel-PVB composites', *J. Mater. Sci.*, 2003, **38**, pp. 1961–1966
[19] Zhao J.J., Duan Y.Y., Wang X.D., *ET AL.*: 'Radiative properties and heat transfer characteristics of fiber-loaded silica aerogel composites for thermal insulation', *Int. J. Heat Mass Transf.*, 2012, **55**, pp. 5196–5204
[20] Xie T., He Y.L., Hu Z.J.: 'Theoretical study on thermal conductivities of silica aerogel composite insulating material', *Int. J. Heat Mass Transf.*, 2013, **58**, pp. 540–552
[21] Seraji M.M., Sameri G., Davarpanah J., *ET AL.*: 'The effect of high temperature sol-gel polymerization parameters on the microstructure and properties of hydrophobic phenol-formaldehyde/silica hybrid aerogels', *J. Colloid Interface Sci.*, 2017, **493**, pp. 103–110
[22] Ge D., Yang L., Li Y., *ET AL.*: 'Hydrophobic and thermal insulation properties of silica aerogel/epoxy composite', *J. Non-Cryst. Solids*, 2009, **355**, pp. 2610–2615
[23] Motahari S., Motlagh G.H., Moharramzadeh A.: 'Thermal and flammability properties of polypropylene/silica aerogel composites', *J. Macromol. Sci. B.*, 2015, **54**, pp. 1081–1091
[24] Randall J.P., Meador M.A., Jana S.C.: 'Tailoring mechanical properties of aerogels for aerospace applications', *ACS Appl. Mater. Interfaces*, 2011, **3**, pp. 613–626
[25] Boday D.J., Keng P.Y., Muriithi B., *ET AL.*: 'Mechanically reinforced silica aerogel nanocomposites via surface initiated atom transfer radical polymerizations', *J. Mater. Chem.*, 2010, **20**, pp. 6863–6865
[26] Schlabach S., Ochs R., Hanemann T., *ET AL.*: 'Nanoparticles in polymer-matrix composites', *Microsyst. Technol.*, 2011, **7**, pp. 183–193
[27] Nastaran N., Jafarsadegh M.: 'Synthesis and characterization of silica aerogel reinforced rigid polyurethane foam for thermal insulation application', *J. Non-Cryst. Solids*, 2017, **461**, pp. 1–11
[28] Li H.Y., Song L.M., Fu Y.Q., *ET AL.*: 'Loads transfer across static electrical phase interfaces in silica aerogel/polymethyl methacrylate composites', *Compos. Sci. Technol.*, 2017, **138**, pp. 169–178
[29] Shahil K.M.F., Balandin A.A.: 'Graphene-multilayer graphene nanocomposites as highly efficient thermal interface materials', *Nano Lett.*, 2012, **12**, pp. 861–867
[30] Md K.I., Ahmed S.: 'Nanocharacterization of interface between natural fiber and polymer matrix: an overview', *Compos. Interfaces*, 2016, **23**, pp. 105–123
[31] Akm S.R., Donald W.R.: 'Evaluation of the geopolymer/nanofiber interfacial bond strength and their effects on mode-I fracture toughness of geopolymer matrix at high temperature', *Compos. Interfaces*, 2017, **24**, pp. 817–831
[32] Sakamoto H., Hatsuda R., Miyamura K., *ET AL.*: 'Plasma separation PMMA device driven by capillary force controlling surface wettability', *Micro Nano Lett.*, 2012, **7**, pp. 64–67
[33] Sujith A., Shebi A., Sudheesh P., *ET AL.*: 'Natural dye-doped poly (methyl methacrylate) microparticles for nonlinear optics', *Micro Nano Lett.*, 2014, **9**, pp. 566–568
[34] Chang T.C., Fuh Y.K., Tu S.X.: 'Screen printed graphite nanoplatelet and nanoparticle composites for thermal interface materials application', *Microsyst. Technol.*, 2017, **23**, pp. 813–819
[35] Mansoor F., Nooshin M.: 'Physical properties, thermal stability, and glass transition temperature of multi-walled carbon nanotube/polypyrrole nanocomposites', *Compos. Interfaces*, 2014, **21**, pp. 737–747
[36] Fazli Y., Kulani E., Khezri K., *ET AL.*: 'PMMA-grafted silica aerogel nanoparticles via in situ SR&NI ATRP: grafting through approach', *Microporous Mesoporous Mater.*, 2015, **214**, pp. 70–79
[37] Sashkina K.A., Gurikov P.A., Ayupova A.B., *ET AL.*: 'Zeolite/silica aerogel composite monoliths and microspheres', *Microporous Mesoporous Mater.*, 2018, **263**, pp. 106–112
[38] Huang S., Ruan X.D., Zou J., *ET AL.*: 'Thermal conductivity measurement of submicrometer-scale silicon dioxide films by an extended micro-Raman method', *Microsyst. Technol.*, 2009, **15**, pp. 837–842
[39] Luo C.H., Wei N., Luo X.F., *ET AL.*: 'Morphology transition of dual-responsive ABC terpolymer in water: effect of hydrophobic block', *Macromol. Chem. Phys.*, 2018, **219**, p. 1800124

doi: 10.1049/mnl.2018.5099